A novel Technique for Sensorless Control of High Power Induction Motors Using Multilevel Converters

K.Saleh
Member

M.Sumner
Senior Member

G.Qiang
Member

G.Asher
Senior Member

Department of Electrical/Electronic Engineering
Faculty of Engineering
University Park
Nottingham
NG7 2RD
eexks4@nottingham.ac.uk

Abstract -- This paper introduces a new scheme to track the rotor slotting saliency in induction motors by using the measurement of current derivatives in response to test vectors imposed during null switching vectors of a standard PWM scheme by using 3 H-bridges connected in series with a 2-Level inverter. The scheme aims to reduce the current distortion usually introduced by applying the sensorless control strategies in 2-Level inverters. The H-Bridges can generate low voltage test vectors which can be used to track the rotor slotting saliency and the same time reduce the distortion in the current directly, as well as shortening the minimum pulse width (t_{min}) which adds a further improvement to current distortion without compromising the quality of the sensorless performance of the system. Moreover, the new technique can work in a wide speed range and its implementation requires only the minimum of control modifications to the operation of the multilevel inverter as the proposed application of this sensorless technique is to high power multilevel converters which use a combination of series connected GTO and IGBT based H-Bridges to achieve a reasonable quality medium voltage waveform for motor drives. Also some automotive drives have recently been proposed which use the same specific topology as used in this work.

***Index Terms*--. Sensorless Control, Multilevel Inverter, INFORM, Fundamental PWM.**

I. INTRODUCTION

Sensorless control of induction motor drives has been widely researched for systems employing standard two level inverters. At low and zero speed, some form of additional excitation such as signal injection [1-2] or pulse based injection [3-5] have been proposed to improve performance. However, these techniques introduce significant additional current distortion, either because of the test signal/pulse itself, or the fact that switching vectors need to be a minimum width for correct measurement of system response. [6] introduced a multilevel INFORM method similar to the 2-level INFORM method [3] to improve the current distortion associated with applying the pulse based or PWM based excitation methods. The method used small excitation (test) voltage generated from separated H-Bridges connected in series with the 2-level inverter as shown in Fig 1. The rotor position is derived from measurement of the motor current derivatives in response to these test voltages. By reducing the excitation voltage, the current distortion can be reduced directly, as well as reducing the minimum vector time (t_{min}) to ensure that the di/dt measurements are settled before sampling.

The limitations of applying such methods are that:-firstly, it can work only at low speeds similar to 2-level INFORM methods [3]; secondly, a control modification to the operation of the multilevel inverter over three successive PWM periods is required each time the rotor position needs to be updated when this method is implemented on the intended applications [7][8]. These limitations are related to the way that test pulses are applied as shown in Fig 2.a (applied over 3 successive PWM periods).

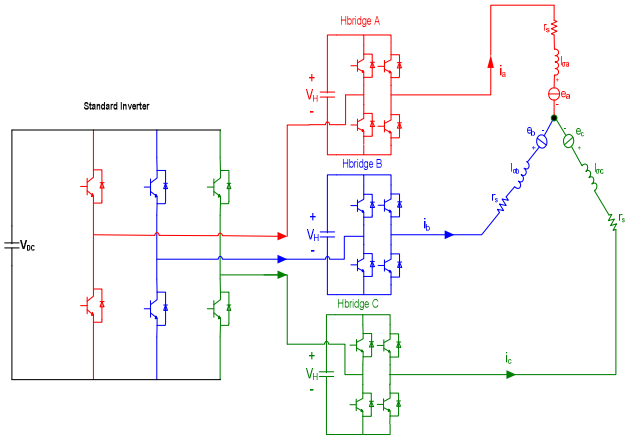

Fig 1. Topology of the prototype multilevel converter

This paper introduces a new method (multilevel modified INFORM method) that takes advantage of reducing the excitation voltage to reduce the current distortion and at the same time overcomes the limitations associated with the multilevel INFORM method [6]. The key point of this improvement is related to the fact that all the test pulses are applied in a single PWM period instead of three PWM periods as shown Fig 2.b which means that the control modification to the operation of the multilevel inverter is needed only in one single PWM period when the rotor position needs to be updated. These improvements make this method more convenient for the intended application in [7][8], and in particular extend the maximum operating speed range.

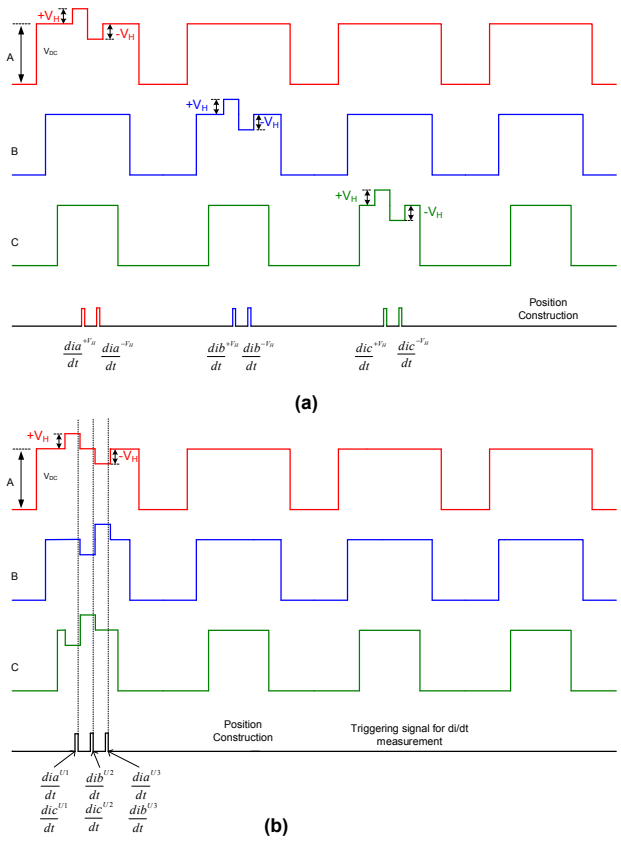

Fig 2.a PWM waveform for the multilevel INFORM method. Fig 2.b PWM waveform for the new method (multilevel modified INFORM method)

II. IMPLEMENTATION OF A SMALL VOLTAGE PULSE USING THE H-BRIDGES

Fig 1 shows the schematic for the multilevel converter developed for this project. Three H Bridges have been connected to a standard inverter. This configuration is designed to evaluate the principle of the method even if it does not use the envisaged target topology. It is however anticipated that the method developed here will be applicable to very high power induction motor drives fed from "isolated cell" multi-level converters which employ different switching devices and cell voltages as proposed in [7][8].

During normal operation, no additional test-pulses are imposed on the machine, and the H-Bridges will have a switching pattern that produces zero volts at their outputs as shown in Fig 3.a i.e. the upper two IGBTs will be ON. When a positive pulse ($+V_H$) is required from a particular H Bridge, to impose a positive "test pulse" on that machine phase winding, the switching pattern of the H-Bridge will be as shown in Fig 3.b. Finally when a negative test-pulse ($-V_H$) is required, the H-Bridge will have a switching pattern as seen in Fig 3.c.

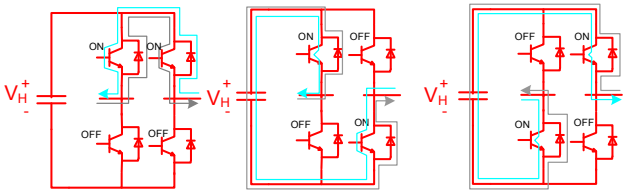

Fig 3.a: H-Bridge switching and current directions to produce 0 V output voltage

Fig 3.b: H-Bridge switching and current directions to produce $+V_H$ V output voltage

Fig 3.c: H-Bridge switching and current directions to produce $-V_H$ V output voltage

III. TRACKING THE ROTOR SLOTTING SALIENCY

The stator leakage inductances of the induction motor are modulated by anisotropy either from the rotor slotting or from the saturation of the main flux. The modulation can be expressed by the following equations:-

$$l\sigma a = L_0 + \Delta L\cos(n_{an}\theta_{an}) \quad (1)$$

$$l\sigma b = L_0 + \Delta L\cos\left(n_{an}(\theta_{an} - \frac{2\pi}{3}\right) \quad (2)$$

$$l\sigma c = L_0 + \Delta L\cos\left(n_{an}(\theta_{an} - \frac{4\pi}{3}\right) \quad (3)$$

Where L_0 is the average inductance and ΔL is the variation of leakage inductance due to the rotor anisotropy (n_{an}=2 for saturation anisotropy , and $n_{an} = \frac{N_r}{p}$ for rotor slotting , where N_r is the rotor slot number and p is the number of pole pairs).

The modulation of the stator leakage inductances can be seen in the transient response of the motor line current to the test vectors imposed by the H-Bridges shown in Fig 2.b. By measuring the transient current (di/dt) in response to the test vector it is possible to detect the inductance variation and track the rotor position.

Tracking the rotor slot position using this method can be achieved by taking three cases in which three different switching states U1, U2, U3 are applied to the motor terminals.

Case 1 : for case 1, the switching state U1 is imposed i.e. H-Bridge A generates $+V_H$, while H-Bridge B generates 0 V, and H-Bridge C generates $-V_H$. The equivalent circuit for the three phase induction motor with applied switching state (U1) is shown in Fig 4.

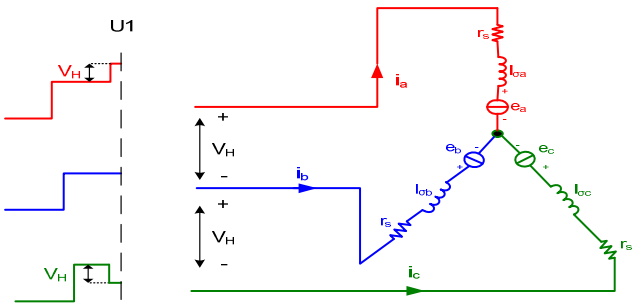

Fig.4 Stator circuit when the H-Bridges generate U1.

Using the circuit of Fig. 4. the following equations can be derived:-

$$+V_H = \overbrace{r_s i_a + l_{\sigma a}\frac{di_a}{dt} + e_a - r_s i_b - l_{\sigma b}\frac{di_b}{dt} - e_b}^{(U1)} \quad (4)$$

$$+V_H = \overbrace{r_s i_b + l_{\sigma b}\frac{di_b}{dt} + e_b - r_s i_c - l_{\sigma c}\frac{di_c}{dt} - e_c}^{(U1)} \quad (5)$$

$$-2V_H = \overbrace{r_s i_c + l_{\sigma c}\frac{di_c}{dt} + e_c - r_s i_a - l_{\sigma a}\frac{di_a}{dt} - e_a}^{(U1)} \quad (6)$$

where the superscript $^{(U1)}$ denotes that the measurement is made during the imposition of the U1 switching state .

Case 2 :- switching state U2 is imposed i.e. H-Bridge A generates 0 V, while H-Bridge B generates -V_H , and H-Bridge C generates +V_H , The equivalent circuit for the three phase induction motor with applied switching state U2 is shown in Fig 5.

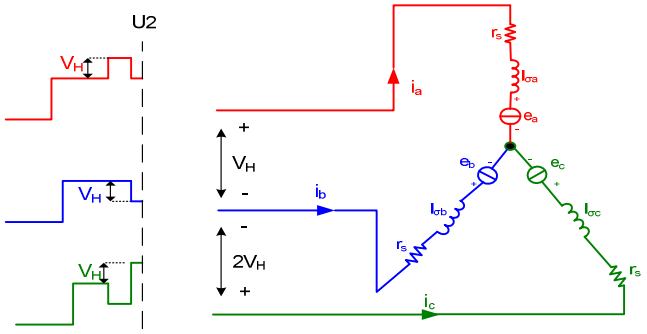

Fig 5.Stator circuit when H-Bridges generate U2

From the circuit of Fig. 5. the following equations can be derived:-

$$V_H = \overbrace{r_s i_a + l_{\sigma a}\frac{di_a}{dt} + e_a - r_s i_b - l_{\sigma b}\frac{di_b}{dt} - e_b}^{(U2)} \quad (7)$$

$$-2V_H = \overbrace{r_s i_b + l_{\sigma b}\frac{di_b}{dt} + e_b - r_s i_c - l_{\sigma c}\frac{di_c}{dt} - e_c}^{(U2)} \quad (8)$$

$$+V_H = \overbrace{r_s i_c + l_{\sigma c}\frac{di_c}{dt} + e_c - r_s i_a - l_{\sigma a}\frac{di_a}{dt} - e_a}^{(U2)} \quad (9)$$

Case 3:- switching state U3 is imposed i.e. H-Bridge A generates -V, while H-Bridge B generates +V, and H-Bridge C generates 0 V. The equivalent circuit for the three phase induction motor with applied switching state U3 is shown in Fig 6.

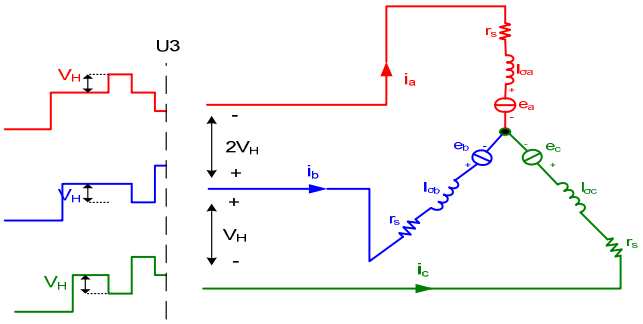

Fig.6 Stator circuit when the H-Bridges generate U3.

From the circuit of Fig. 6. the following equations can be derived:-

$$+V_H = \overbrace{r_s i_a + l_{\sigma a}\frac{di_a}{dt} + e_a - r_s i_b - l_{\sigma b}\frac{di_b}{dt} - e_b}^{(U3)} \quad (10)$$

$$+V_H = \overbrace{r_s i_b + l_{\sigma b}\frac{di_b}{dt} + e_b - r_s i_c - l_{\sigma c}\frac{di_c}{dt} - e_c}^{(U3)} \quad (11)$$

$$-2V_H = \overbrace{r_s i_c + l_{\sigma c}\frac{di_c}{dt} + e_c - r_s i_a - l_{\sigma a}\frac{di_a}{dt} - e_a}^{(U3)} \quad (12)$$

By subtracting the equations for case 3 (when U3 is applied) from the related equations for case 1 (when U1 is applied) with the assumptions that

1) the voltage across the stator resistance is small and can be neglected compared to the applied voltage.
2) There is little change between switching states in term of time separation.

the following equations can be obtained:-

$$+3V_H = l_{\sigma a}\left(\frac{\overbrace{di_a}^{(U1)}}{dt} - \frac{\overbrace{di_a}^{(U3)}}{dt}\right) - l_{\sigma b}\left(\frac{\overbrace{di_b}^{(U1)}}{dt} - \frac{\overbrace{di_b}^{(U3)}}{dt}\right) \quad (13)$$

$$0 = l_{\sigma b}\left(\frac{\overbrace{di_b}^{(U1)}}{dt} - \frac{\overbrace{di_b}^{(U3)}}{dt}\right) - l_{\sigma c}\left(\frac{\overbrace{di_c}^{(U1)}}{dt} - \frac{\overbrace{di_c}^{(U3)}}{dt}\right) \quad (14)$$

$$\boldsymbol{-3V_H = l_{\sigma c}\left(\frac{\overbrace{di_c}^{(U1)}}{dt} - \frac{\overbrace{di_c}^{(U3)}}{dt}\right) - l_{\sigma a}\left(\frac{\overbrace{di_a}^{(U1)}}{dt} - \frac{\overbrace{di_a}^{(U3)}}{dt}\right)} \quad (15)$$

Multiplying (13) by $l_{\sigma c}$ and (15) by $l_{\sigma b}$ respectively and subtracting one from the other yields :-

$$\left(\frac{\overbrace{di_a}^{(U1)}}{dt} - \frac{\overbrace{di_a}^{(U3)}}{dt}\right) = \frac{+3V(l_{\sigma b} + l_{\sigma c})}{(l_{\sigma a}\, l_{\sigma b} + l_{\sigma b} l_{\sigma c} + l_{\sigma c} l_{\sigma a})} \quad (16)$$

And substituting $l_{\sigma a}\, l_{\sigma b} + l_{\sigma b} l_{\sigma c} + l_{\sigma c} l_{\sigma a}$ by

$3L_0\left(1-\left(\frac{\Delta L}{2L_0}\right)^2\right)$ yields:-

$$\left(\frac{\overset{(U1)}{\widehat{di_a}}}{dt}-\frac{\overset{(U3)}{\widehat{di_a}}}{dt}\right)=\frac{3V(2L_0-\Delta L cos(n_{an}\theta_{an}))}{3L_0\left(1-\left(\frac{\Delta L}{2L_0}\right)^2\right)} \quad (17)$$

By assuming that $h=\frac{3\left(1-\left(\frac{\Delta L}{2L_0}\right)^2\right)}{3V}$ is constant, the position scalar – the variation with respect to $n_{an}\theta_{an}$ P_a - for the rotor slot position can be defined as:-

$$P_a = 2 - h\left(\frac{\overset{(U1)}{\widehat{di_a}}}{dt}-\frac{\overset{(U3)}{\widehat{di_a}}}{dt}\right) \quad (18)$$

The process of (13),(14),(15) can be repeated using the other combinations U1,U2 and U2,U3 so that the other position scalars can be defined:-

$$P_b = 2 - h\left(\frac{\overset{(U3)}{\widehat{di_b}}}{dt}-\frac{\overset{(U2)}{\widehat{di_b}}}{dt}\right) \quad (19)$$

$$P_c = 2 - h\left(\frac{\overset{(U2)}{\widehat{di_c}}}{dt}-\frac{\overset{(U1)}{\widehat{di_c}}}{dt}\right) \quad (20)$$

The final form for the α and β components of the rotor slot position scalar will be:-

$$P_\alpha = P_a + \frac{1}{2}(P_b + P_c) \quad (21)$$

$$P_\beta = \frac{\sqrt{3}}{2}(P_b - P_c) \quad (22)$$

The slot passing angle will be obtained from arc tan (P_β/P_α). By using this method, the rotor slotting position can be estimated by measuring the current derivative of the test vector shown in Fig 2.b without the need for any motor parameter or any constants.

IV. ROTOR POSITION ESTIMATION

The anisotropy caused by the rotor slotting was tracked using the proposed method i.e. measuring di/dt in response to the test vector sequence of Fig. 2.b. The position signals $P\alpha$ and $P\beta$ derived for the experimental system described in the previous section obtained using (21) and (22) are show in Fig. 7.

The rotor slotting saliency $(14\,f_r)$ is clear, but other disturbance harmonics are present which distort the position estimate. The $(2f_e)$ and (f_e) components are due to the saturation in the machine and the unbalance in the di/dt sensors respectively and the component $(14f_r + 2f_e)$ arises because the position signal $(14f_r)$ is modulated by saturation in the machine $(2f_e)$.

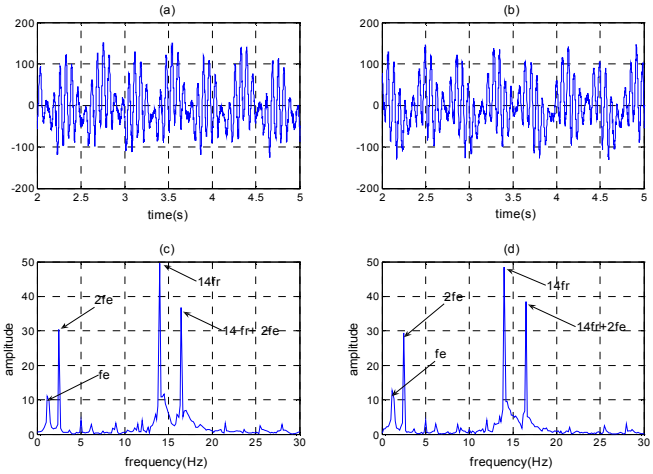

Fig 7 (a) and (b): α and β components of the estimated position signal at 30 rpm ,50% load. (c) and (d): Frequency spectrum of α and β components of the estimated position.

The disturbance elemination method proposed in [10] is used to remove the $(2f_e)$ and (f_e) . This method assumes that these components will vary due to the load conditions only, and is independent of the speed. The disturbance at $(14f_r + 2f_e)$ is removed by using the sideband filter in the rotating frame $14\theta_r + 2\theta_e$ proposed in [10] as shown in fig. 8.

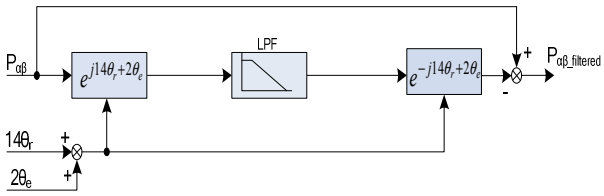

Fig 8: Schematic of the side band filter.

The position signals after filtering are shown in Fig. 9. It can be seen that the rotor slotting effect is now much stronger and is now suitable for rotor position tracking.

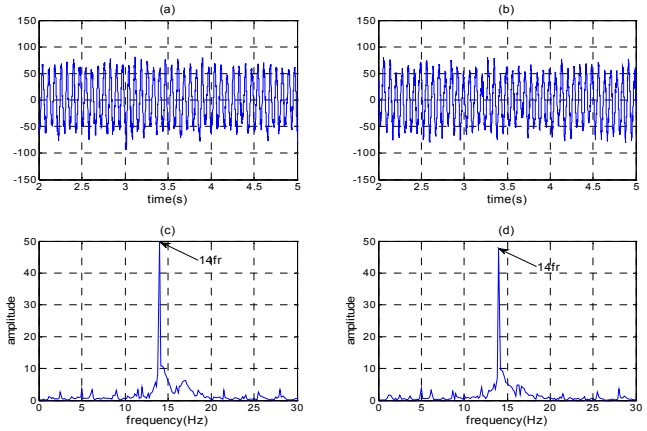

Fig 9 (a) and (b): filtered α and β component of the estimated position at 30 rpm ,50% load. (c) and (d): FFT of α and β components of the estimated position.

The quality of the estimated position signal shown in the figure above is good enough to be used in a complete sensorless system as will be described in the next section.

V. Experimental Results

The proposed method has been implemented on a squirrel cage, star connected, 4 pole, 16kW, 50Hz induction motor with 28 semi-closed, non-skewed rotor slots. The switching frequency of the main Inverter was 5 kHz, and the H-Bridge DC link voltage used in the experiment was 150V for the multilevel INFORM method and 100V in the multilevel modified INFORM method. The reason for applying smaller H-Bridge DC link voltages in the new method is that 2 H-Bridges in two different lines were switched at the same time which increases the amplitude of the di/dt signal and makes the Signal to Noise Ratio (SNR) of the estimated position in the two methods same. The width of the H-Bridge test vectors were 20 us and the rated current for the H-Bridges was 70% of the machine rated load and so the maximum safe load that can be applied to the machine is 50% of the rated load.

A. *Fully Sensorless Speed Control*

After filtering the raw position signals from the disturbances, the α and β component of this position signal is used with the mechanical observer described in [12]. The estimated rotor position and speed are then used for field orientation and speed feedback for a sensorless speed control system as shown in Fig 10.

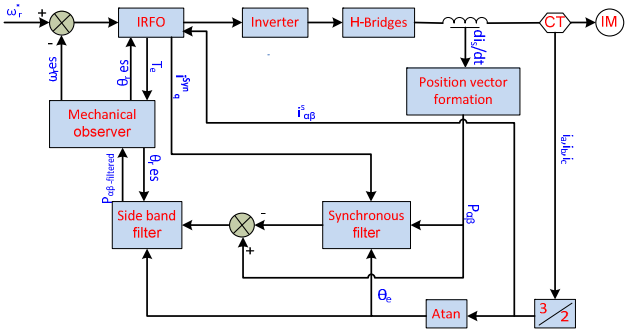

Fig 10: System setup of the sensorless speed control

Figures 11, 12, and 13 show the results of full sensorless speed control under no load and loaded conditions using the proposed method. In Fig 11 a speed step change from 350 to 0 back to 350 rpm at no load was demanded to show the method works over a wide speed range. The estimated speed and position seen in the figure proved that the system responded to the speed steps with good dynamic response and good steady state behaviour. Figure 12 shows speed step changes between 350 and 0 rpm with 50% load applied to the system. Again the speed measured from the encoder shows that the fully sensorless system has a very good speed response, even under load.

Fig 13 shows the system response to a load steps between 0 and 50% load. The motor took 0.5 seconds to recover.

The results show that the system can work successfully in full sensorless speed control mode.

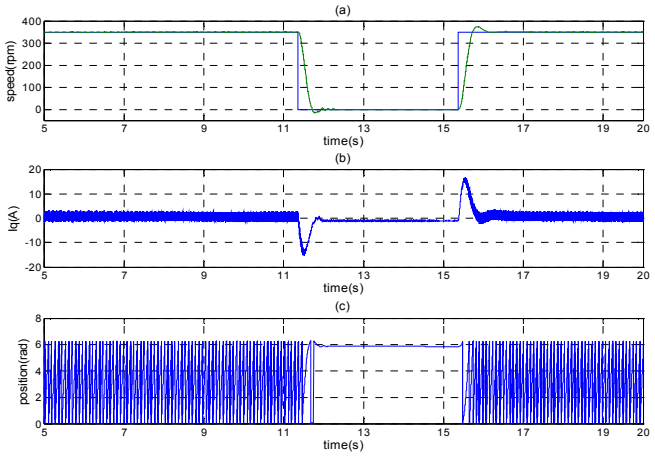

Fig 11 Fully sensorless speed control at no load using the proposed method. (a): reference speed and measured speed, (b): Iq. (c): measured rotor position (blue).

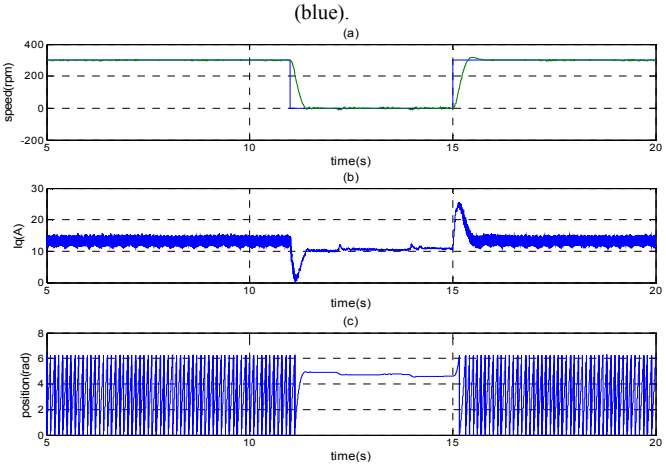

Fig 12: Fully sensorless speed control at 50% Load using the proposed method. (a): measured speed. (b): Iq. (c): measured rotor position.

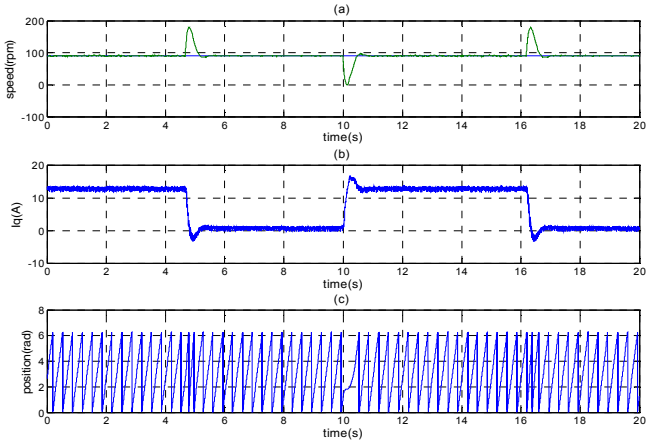

Fig 13: Load steps between 50% and 0 load using the proposed method (a): measured speed and reference speed. (b): Iq. (c): measured rotor position in blue and estimated rotor position in green.

B. Improvement in current distortion

To demonstrate the improvement in the current distortion obtained by applying the new scheme (the multilevel modified INFORM method) compared to those obtained by applying the multilevel INFORM method and both the 2-Level INFORM method and 2-Level Fundamental PWM method, these methods were implemented experimentally on the experimental rig using *sensored* control with two different loads and speeds. The current waveforms associated with applying these methods in addition to the waveforms from operation with no excitation were captured using an oscilloscope and current sensors [13][14] and the Total Harmonic Distortion (THD) was calculated offline. The H bridge excitation voltage used was 150 V for the multilevel INFORM method and 100 V for the multilevel modified INFORM method and the main inverter DC link voltage was 620V, particularly relevant for the 2-level INFORM method and the 2-level fundamental PWM method. The H bridge excitation voltages helped to reduce the minimum pulse width (t_{min}) from 25 µs in the 2-level methods to 20 µs in the multilevel methods.

1- 30 rpm at 35 % load

Fig 14 shows the current wave forms measured while applying the different methods. The spectra for these currents and the THD calculation are shown in Fig 15 and Fig 16 respectively. The results shows that the THD was reduced from 6% and 3.8% in the 2-level INFORM method and the 2-level fundamental PWM method respectively to 1.2% and 1.3% using the multilevel INFORM and modified INFORM methods respectively. This improvement can be noticed also from the reduction in the audible noise level that is achieved by applying the multilevel methods. The difference in THD between the multilevel INFORM method and the multilevel modified INFORM method is due to the fact that two H-Bridges are switched at the same time during the application of the test vectors in the multilevel modified INFORM method while only one H-Bridge is switched during each test vector in the multilevel INFORM method.

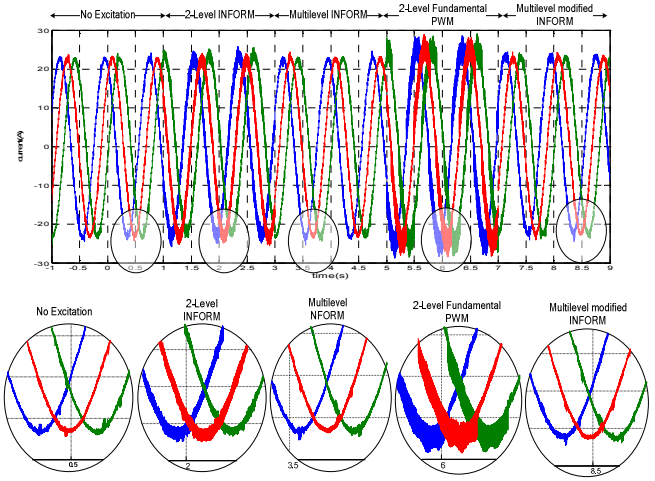

Fig 15 Current waveforms in different excitation methods at 30 rpm and 35% load.

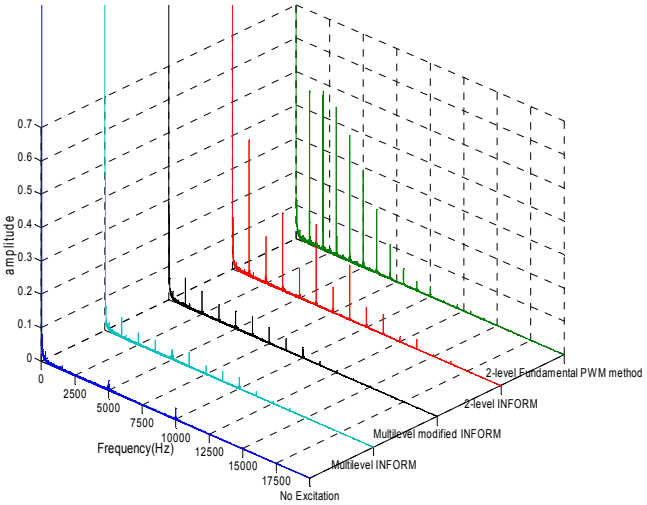

Fig 16 current spectra for different excitation methods at 30 rpm 35% load

Speed= 30 rpm , 35% Load				
2-level Fundamental PWM method	2-level INFORM method	No Excitation	Multilevel INFORM method	Multilevel modified INFORM method
6%	3.8%	1.04%	1.2%	1.3%

Table 1: THD of line current for different excitation methods at 30 rpm and at35% load

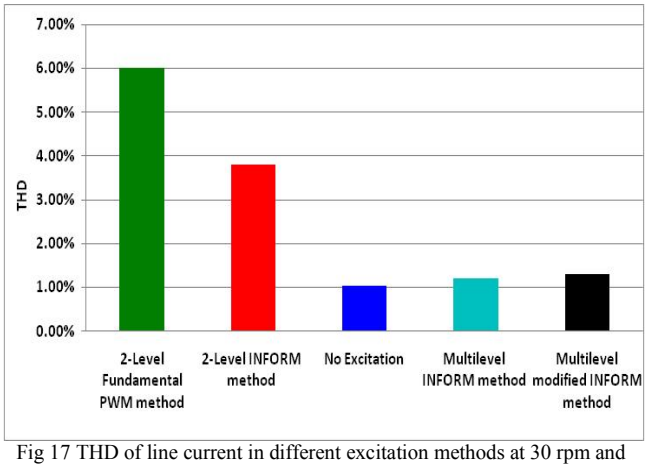

Fig 17 THD of line current in different excitation methods at 30 rpm and 35% load

2- 150 rpm and No load

This test is similar to the previous one except on that motor is running at 150 rpm and at no load. The results in this test are similar to the previous one in terms of the improvement in the current distortion that is achieved by applying the new method. The difference in the THD calculations in this test from previous test is related to the fact that the amplitude of the fundamental component of the current in the previous one is larger because of the machine loading and also because of the rotor slotting harmonics in the current becomes more influent in this speed range.

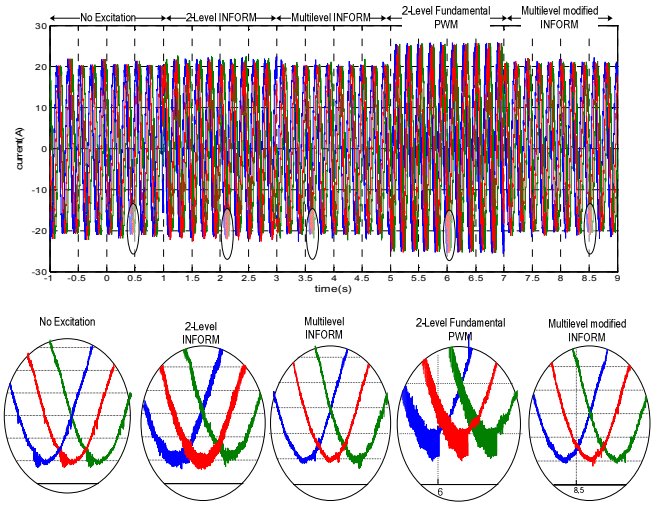

Fig 18. Current waveforms in different excitation methods at 150 rpm and no load.

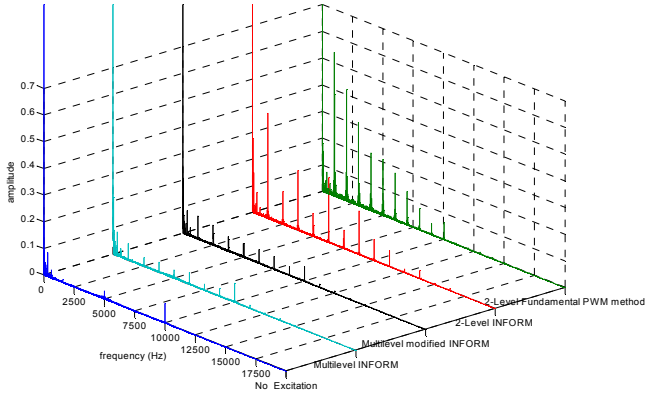

Fig 19 current spectra for different excitation methods at 150 rpm and no load.

Speed= 150 rpm , No Load				
2-level Fundamental PWM method	2-level INFORM method	No Excitation	Multilevel INFORM method	Multilevel modified INFORM method
7.5%	5%	1.37%	1.8%	1.9%

Table 2: THD of line current for different excitation methods at 150 rpm and no load

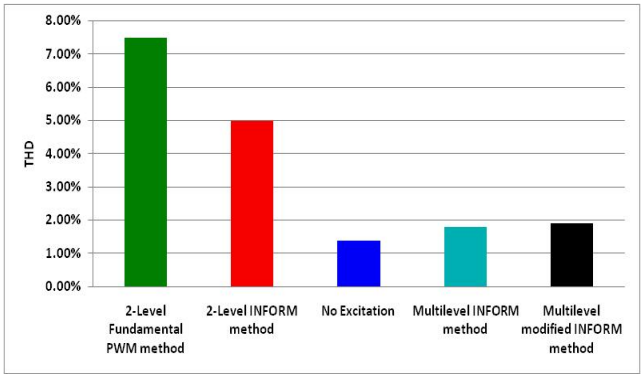

Fig 20 THD of line current in different excitation methods at 150 rpm and no load

C. Improvement in position estimation at higher speeds

By measuring the di/dt due to the test voltages U1, U2 and U3, the saliency can be tracked according to (21-22). In general, for correct position estimation, the time separation between the instants of sampling Pa, Pb and Pc should be as short as possible to make sure that the real rotor slot position does not change too much. According to Fig 2.a, the time separation between sampling Pa and Pc is 400 us. During this period the rotor will rotate 34° if the speed of rotor is 500 rpm and the multilevel INFORM method of Fig. 2.a is used, while the rotor will rotate only 3.4° if the multilevel modified INFORM method of Fig 2.b is used, as illustrated in Fig 21. This 34° movement of the rotor slot causes an error of constructing the α and β components of the estimated slot position as seen in Fig 22 and this leads to an error in rotor slot position estimation. Fig 23 shows that the new method does not have this error and hence the rotor slot position and speed can be estimated without error at this speed. Fig 24 shows the fully sensorless speed control using the new method at no load. It can be seen clearly that a precise sensorless speed control using the new method can be obtained over a wide speed range which is not achievable by the multilevel INFORM method [10].

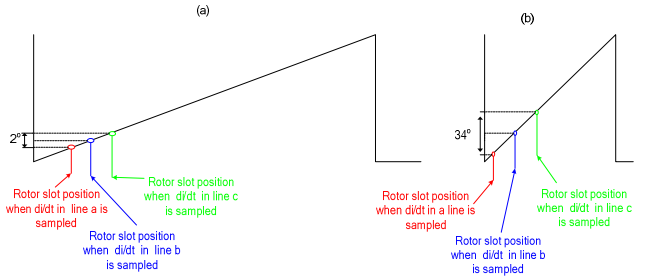

Fig 21 illustration of the sampling rotor slot position components at 500 rpm in (a) the multilevel modified INFORM method (b) the multilevel INFORM method

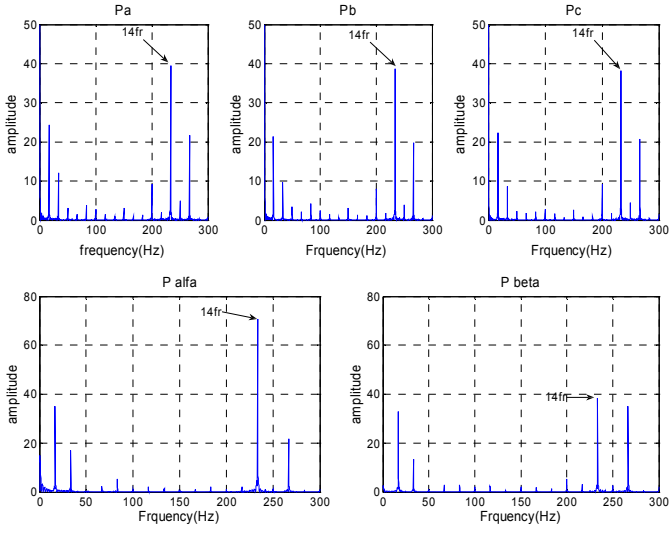

Fig 22 Rotor slot position estimation at 500 rpm for the multilevel INFORM method.

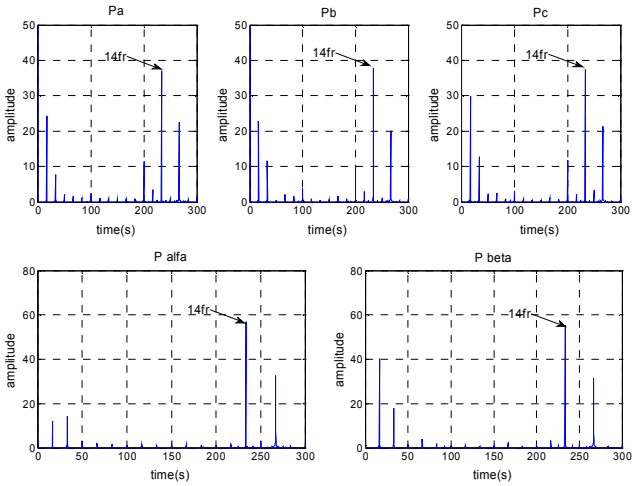

Fig 23 Rotor slot position estimation at 500 rpm for the multilevel modified INFORM method.

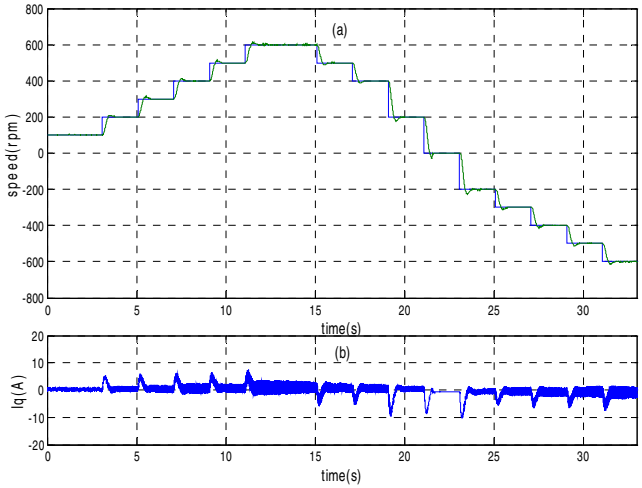

Fig 24 Sensorless speed steps under no load using the multilevel modified INFORM method (a) measured speed and reference speed.(b): Iq.

CONCLUSION

This paper has outlined a new scheme for reducing the current distortion introduced into induction motor drives by low speed sensorless control techniques. The sensorless scheme estimates the rotor position by using low voltage H-Bridges connected in series with a standard two level inverter to generate low voltage test vectors. By reducing the test vector size from 620V (standard DC link voltage to 100V (H-Bridge DC link) the current ripple associated with the minimum active pulse width extension is reduced, although it will also have an effect on the di/dt measurement i.e. decrease the signal to noise ratio (SNR). This challenge is overcome by using the new di/dt sensors introduced in [9]. Experimental results show that the new multilevel sensorless method achieves a significant improvement to the THD of the motor current, reducing it from 6% and 3.8% (2 level fundamental PWM method and the INFORM method respectively) to 1.9% when the new sensorless technique is used. The experimental results also demonstrate the correct control behaviour of the fully speed sensorless control at low and higher speeds at different load conditions. Compared to the multilevel INFORM method [6], the modified multilevel INFORM method has a slightly higher current distortion, higher speed operation, and is more convenient to apply to a true cascade H-Bridge multilevel inverter structure with the ability to get the same saliency amplitude using a smaller excitation voltage. The paper has demonstrated the viability of using additional H bridges for sensorless induction motor control. The cost of this approach will be prohibitive for low to medium power drives. However, high power induction motors are now being constructed using multi-level inverters, and therefore the techniques described here are very suitable to this class of motor drives.

REFERENCES

[1] P.L.Jansen, R.D.Lorenz," Transducerless Position and Velocity Estimation in Induction and Salient AC Machines", IEEE Transactions on Industry Applications, vol.31, pages:240–247, Mar, 1995.

[2] M.Linke, R.Kennel, J.Holtz, "Sensorless Speed and Position Control of Synchronous Machines using Alternating Carrier Injection", IEEE International Electric Machines and Drives Conference IEMDC03, vol.2, pages:1211–1217, 2003.

[3] M. Schroedl. "Sensorless Control of AC Machines at Low Speed and Standstill Based on the INFORM Method". IEEE IAS Annual Meeting, volume 4, pp. 270-277, (1996).

[4] J. Holtz, J. Juliet."Sensorless Acquisition of the Rotor Position Angle of Induction Motors With Arbitrary Stator Windings". IAS Annual Meeting, volume 2, pp.1675-1682, (2004).

[5] G.Qiang, G.M.Asher, M.Sumner.M, P.Makys. "Position Estimation of AC Machines at all Frequencies Using Only Space Vector PWM based Excitation", 3rd IET International Conference , pp. 61-70, (2006).

[6] K.Saleh, G.M.Asher, M.Sumner, M.Tomasini, G.Qiang. "Low Speed Sensorless Control of an Induction Motor Fed by Multilevel Converter to Reduce Current Distortion", EPE 2009 in Barcelona.

[7] M.D.Manjrekar, P.K.Steimer, T.A.Lipo," Hybrid Multilevel Power Conversion System: A competitive Solution for High-Power Applications", IEEE transactions on industry applications, volume 36, pp 834 – 841, (2000)

[8] H.Liu, L.M.Tolbert, S.Khomfoi, B.Ozpineci, Z.Du, "Hybrid Cascaded Multilevel Inverter with PWM Control Method", IEEE Power Electronics Specialists Conference, pages:162-166, June,2008.

[9] M.Tomasini , S.Bolognani, "Innovative control algorithms for electric drives – Time optimal current and torque control of IPM SM drives and experimental rig to test a rotor anisotropy-based sensorless vector control of IM drives", PhD thesis, University of Padua, Italy, (2007).

[10] P.Makys, G.M.Asher, M.Sumner ,Q.Gao, J.Vittek. "A low Memory Disturbance Elimination Method for Sensorless Control of Induction Motor Drive Using Test Vector Injection" ,IECON 2006,pp.1071-1076 .

[11] J. Holtz,H. Pan, "Elimination of Saturation Effects in Sensorless Position Controlled Induction Motors", IEEE transaction in industrial application, volume 40, pp.623-631, (2000).

[12] R.D. Lorenz , K.W. Van Patten. "High-Resolution Velocity Estimation for All-Digital, ac Servo Drives" , IEEE transactions on industry applications, volume 27, pp.701 – 705, (1991).

[13]www.lecroy.com/tm/products/scopes/WaveRunner_6000A/WR6A_DC.pdf

[14]www.lecroy.com/tm/products/probes/current/current_probes_datasheet.pdf